Supercritical dynamics at the edge-of-chaos underlies optimal decision-making

Journal of Physics: Complexity

OPEN ACCESS

RECEIVED
27 July 2021

REVISED
21 October 2021

ACCEPTED FOR PUBLICATION
17 November 2021

PUBLISHED
1 December 2021

PAPER

Supercritical dynamics at the edge-of-chaos underlies optimal decision-making

Adrián F Amil[1,2] **and Paul F M J Verschure**[1,3,*]

[1] Institute for Bioengineering of Catalonia (IBEC), Barcelona, Spain
[2] Universitat Pompeu Fabra (UPF), Barcelona, Spain
[3] Catalan Institution for Research and Advanced Studies (ICREA), Barcelona, Spain
[*] Author to whom any correspondence should be addressed.

E-mail: pverschure@ibecbarcelona.eu

Keywords: supercriticality, edge-of-chaos, attractor model

Abstract

Critical dynamics, characterized by scale-free neuronal avalanches, is thought to underlie optimal function in the sensory cortices by maximizing information transmission, capacity, and dynamic range. In contrast, deviations from criticality have not yet been considered to support any cognitive processes. Nonetheless, neocortical areas related to working memory and decision-making seem to rely on long-lasting periods of ignition-like persistent firing. Such firing patterns are reminiscent of supercritical states where runaway excitation dominates the circuit dynamics. In addition, a macroscopic gradient of the relative density of Somatostatin (SST+) and Parvalbumin (PV+) inhibitory interneurons throughout the cortical hierarchy has been suggested to determine the functional specialization of low- versus high-order cortex. These observations thus raise the question of whether persistent activity in high-order areas results from the intrinsic features of the neocortical circuitry. We used an attractor model of the canonical cortical circuit performing a perceptual decision-making task to address this question. Our model reproduces the known saddle-node bifurcation where persistent activity emerges, merely by increasing the SST+/PV+ ratio while keeping the input and recurrent excitation constant. The regime beyond such a phase transition renders the circuit increasingly sensitive to random fluctuations of the inputs—i.e., chaotic—, defining an optimal SST+/PV+ ratio around the edge-of-chaos. Further, we show that both the optimal SST+/PV+ ratio and the region of the phase transition decrease monotonically with increasing input noise. This suggests that cortical circuits regulate their intrinsic dynamics via inhibitory interneurons to attain optimal sensitivity in the face of varying uncertainty. Hence, on the one hand, we link the emergence of supercritical dynamics at the edge-of-chaos to the gradient of the SST+/PV+ ratio along the cortical hierarchy, and, on the other hand, explain the behavioral effects of the differential regulation of SST+ and PV+ interneurons by acetylcholine in the presence of input uncertainty.

1. Introduction

Self-organized criticality, as characterized by power-law scaling of neuronal avalanches, occurs as a continuous second-order phase transition [1], and has been proposed as a hallmark of optimal function in cortical networks [2]. Concretely, theoretical and *in vitro* studies first showed that, by achieving a controlled propagation of spiking activity through excitatory–inhibitory balance, circuits in such a critical regime maximize the transfer of information [3], pattern generation [3], and dynamic range [4]. Further, *in vivo* studies later confirmed that early sensory areas in the cortex lie in criticality and suggested that such critical regime is actively maintained through homeostatic inhibitory mechanisms [5]. In contrast, subcritical or supercritical regimes—where the population response tends to wane or saturate, respectively—have rarely been considered to underlie any cognitive processes (but see an exception about the role of supercriticality for effective information transmission

in [6, 7]). Nevertheless, physiological evidence suggests that saturated population responses characterized by persistent firing indeed play a role in making perceptual decisions [8], and maintaining information over time [9] while broadcasting it to the rest of the brain [10]. Hence, this type of population-level persistent firing could arise either from outer feedback loops with other cortical or subcortical areas, or from the intrinsic features of the local neocortical microcircuitry. Notably, although increased recurrent excitation—through the higher density of *N*-methyl-d-aspartate, or NMDA, receptors in pyramidal dendrites [11, 12]—has been hypothesized to be the key feature giving rise to distinct dynamics and function in low- and high-order cortical areas, a recently reported macroscopic gradient of increasing Somatostatin-to-Parvalbumin (SST+/PV+) ratio along the sensory hierarchy has been suggested to play a key role as well [13]. This suggests that the SST+/PV+ gradient might be a key feature determining whether the local circuits throughout the cortical hierarchy have critical or supercritical dynamics, which in turn would dictate their respective functions during information processing.

In sensory areas, the cortical circuit is dominated by PV+ soma-targeting interneurons, which provide shared inhibitory feedback, keeping pyramidal cells in a low and sparse firing rate regime and implementing a form of gain control [14]. In contrast, frontal cortical circuits are dominated by SST+ dendritic-targeting interneurons, which appear to impose competitive dynamics between pyramidal populations via excitatory–inhibitory and inhibitory–inhibitory projections (i.e., self-disinhibition), effectively controlling mutual inhibition and affording persistent activity of the winning population [15, 16]. Notably, recent physiological evidence has shown that different plasticity rules governing PV+ and SST+ interneurons support their respective functional roles, with PV+ providing homeostatic control of the firing rates of excitatory assemblies, and SST+ consolidating lateral inhibition and competition between the assemblies [17]. In addition, local circuit dynamics have been demonstrated to be under the control of neuromodulators like acetylcholine (ACh). Concretely, ACh differentially regulates the excitability and firing of SST+ and PV+ interneurons [18]. In turn, the induction of cholinergic transients has also been shown to increase the false alarm rates in mice performing a signal detection task [19], thus demonstrating its key role in shaping the circuit dynamics related to perceptual decision-making. Furthermore, ACh has been linked to uncertainty estimation of inputs—i.e., input variance—during perceptual decisions [20]. Hence, we suggest that ACh might play a crucial role in modulating the population dynamics of neocortical microcircuits according to input uncertainty by differentially regulating mutual and feedback inhibition throughout the cortical hierarchy.

In this paper, we used a computational model of the cortical microcircuit to test the hypothesis that supercritical dynamics can emerge in high-order areas due to an increasing SST+/PV+ gradient and that the transition to the supercritical regime can be further controlled locally by ACh-like neuromodulation of the inhibitory interneurons.

2. Results

To test the hypothesis that supercriticality arises from the intrinsic features of the neocortical circuitry, we used an attractor model of the canonical cortical circuit that includes populations of excitatory neurons with recurrent connections and driven by external inputs, as well as the inhibitory effects of populations of SST+ and PV+ interneurons [17] (figure 1(A)). Notably, by incorporating SST+ and PV+ interneurons simultaneously, we combined two features of the neural mass models of decision-making that have typically been considered as interchangeable [21]: mutual and feedback inhibition, respectively. Furthermore, based on previous literature on the role of ACh in shaping SST+ and PV+ responses [18], we were also able to parametrize a trade-off between mutual and feedback inhibition. Hence, the population dynamics—i.e., mean firing rate—of excitatory neurons is determined by the interplay between external inputs—deterministic, or stochastic, depending on experimental condition—, and the ratio between inhibitory SST+ and PV+ populations set by the ACh level. Importantly, and in contrast to previous studies, we kept the recurrent excitation constant and focused on the role of the SST+/PV+ ratio in modulating the dynamics of the circuit (see methods for more details).

We first determined the phase space of the model and how it was shaped by the SST+/PV+ ratio (figure 1(A))—ACh level—, under deterministic, unbiased inputs (i.e., same for both populations). We observed that the typical phase transition from a low firing rate attractor to the bistable regime of persistent activity—a saddle-node bifurcation—could be achieved merely by increasing the ACh level regulating the SST+/PV+ ratio, instead of by increasing the input strength or the recurrent excitation (as done in previous studies, e.g., [22]). Notably, after the phase transition, we can observe how the saddle node progressively moves away from the starting point (figure 1(B)), which magnifies the gradients close to the latter. This effect has notable implications for the input sensitivity of the circuit to random fluctuations, as we demonstrate below.

We then characterized the aforementioned phase transition with a bifurcation diagram (figure 2(A)) and by computing the largest Lyapunov exponents with respect to the initial resting state (figure 2(B)), with the latter

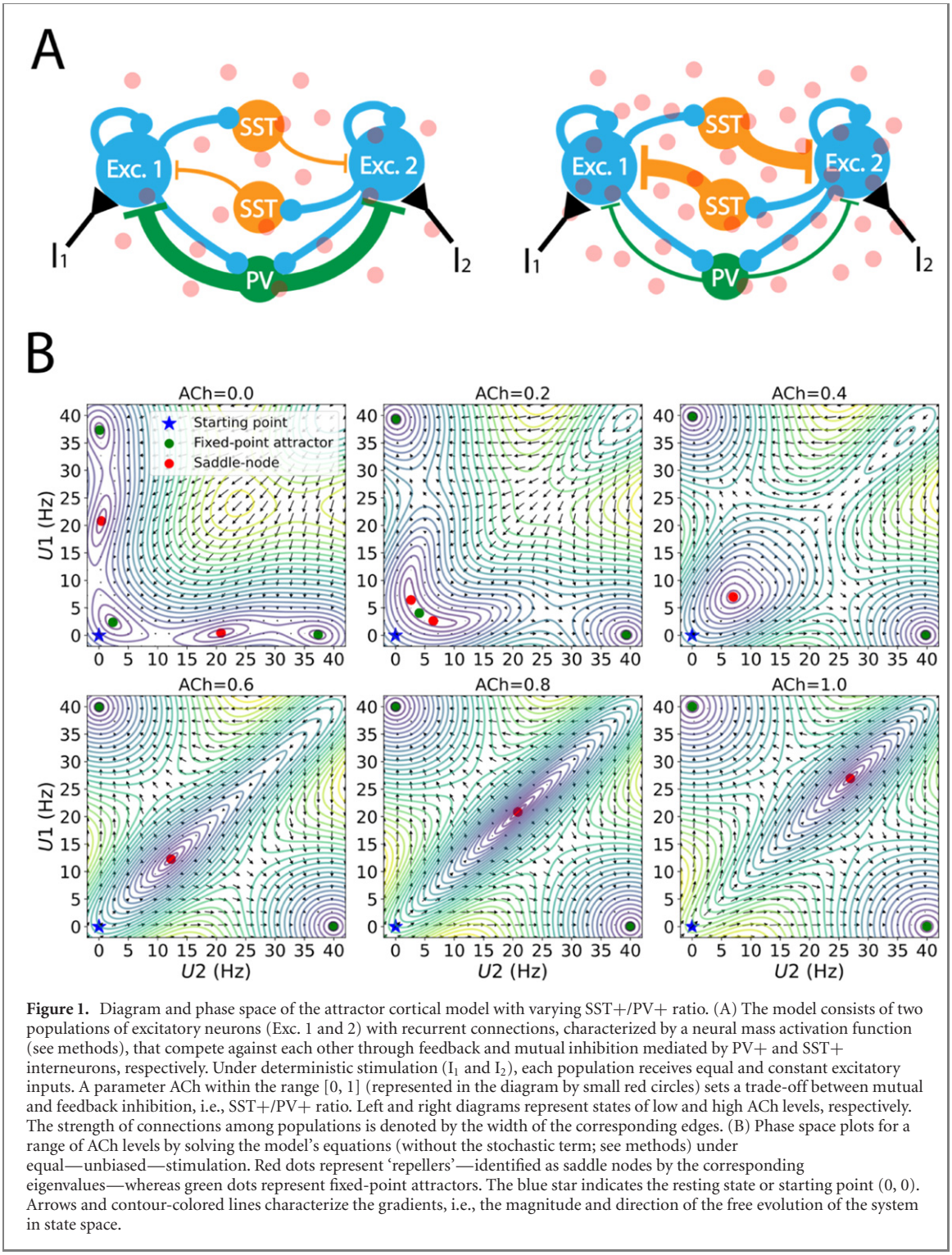

Figure 1. Diagram and phase space of the attractor cortical model with varying SST+/PV+ ratio. (A) The model consists of two populations of excitatory neurons (Exc. 1 and 2) with recurrent connections, characterized by a neural mass activation function (see methods), that compete against each other through feedback and mutual inhibition mediated by PV+ and SST+ interneurons, respectively. Under deterministic stimulation (I_1 and I_2), each population receives equal and constant excitatory inputs. A parameter ACh within the range [0, 1] (represented in the diagram by small red circles) sets a trade-off between mutual and feedback inhibition, i.e., SST+/PV+ ratio. Left and right diagrams represent states of low and high ACh levels, respectively. The strength of connections among populations is denoted by the width of the corresponding edges. (B) Phase space plots for a range of ACh levels by solving the model's equations (without the stochastic term; see methods) under equal—unbiased—stimulation. Red dots represent 'repellers'—identified as saddle nodes by the corresponding eigenvalues—whereas green dots represent fixed-point attractors. The blue star indicates the resting state or starting point (0, 0). Arrows and contour-colored lines characterize the gradients, i.e., the magnitude and direction of the free evolution of the system in state space.

approximating the effects of small random fluctuations—i.e., noise. On the one hand, the bifurcation diagram—representing the last achievable states by the circuit—showed the sudden emergence of the two fixed-point attractors, together with the saddle node in-between them. On the other hand, this saddle-node bifurcation was accompanied by positive, increasing Lyapunov exponents, suggesting that the bistable circuit becomes progressively more sensitive to small perturbations of its initial state as the ACh parameter—SST+/PV+ ratio—is increased. Importantly, this result links the emergence of persistent activity (critical-to-supercritical transition) to the notion of edge-of-chaos by virtue of a saddle-node bifurcation.

To understand the dynamics of the model under more realistic conditions, we simulated a perceptual decision-making task as a stochastic process and added Gaussian noise to the population activity, representing the input variance or uncertainty (figure 3). In turn, the difference in external stimulation between the

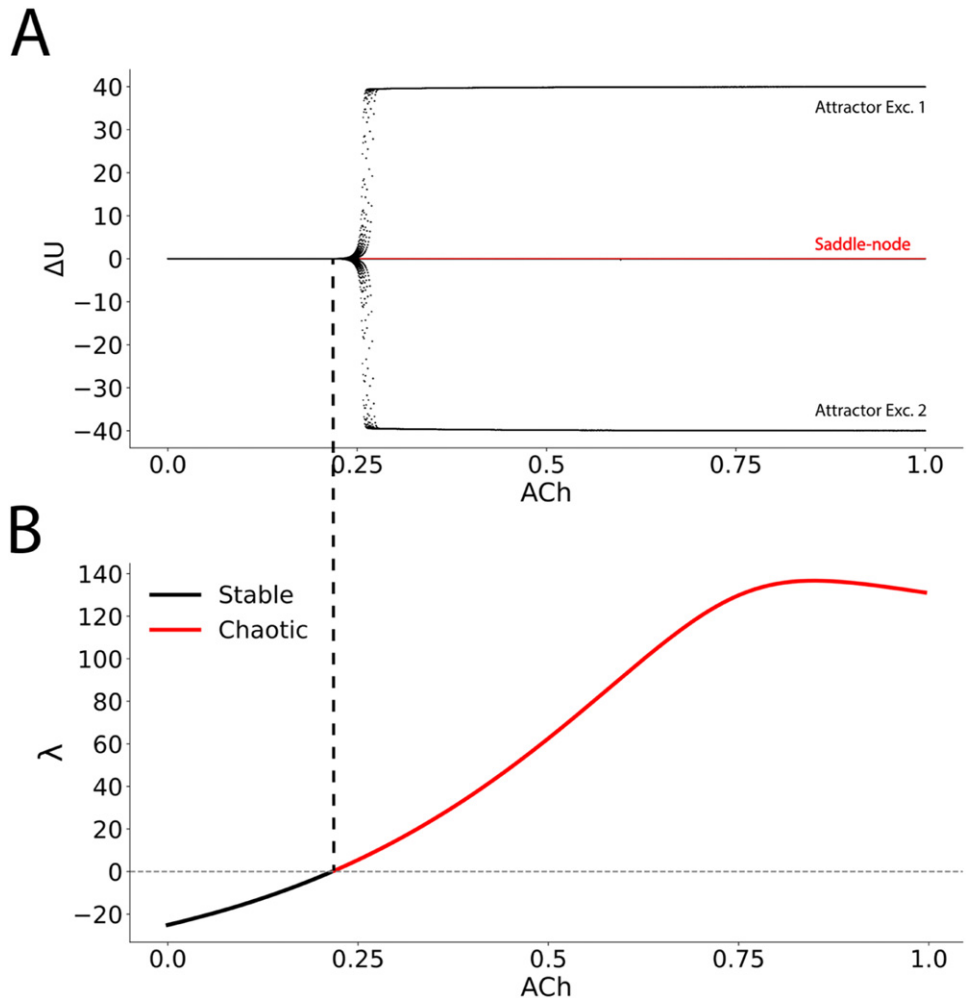

Figure 2. Phase transition to deterministic chaos along the SST+/PV+ gradient. (A) Bifurcation diagram showing the model's final states (ΔU, which is the difference between the resulting populations' firing rates) in the state space across STT+/PV+ ratios—represented by the ACh level. The model is repeatedly evolved from 100 initial values drawn from a 0.01×0.01 rectangular grid, with the starting point (0, 0) as the bottom-left corner of such grid. (B) Largest Lyapunov exponents (λ) across ACh levels, directly computed from the ODE's using the variational matrix approach (see methods). Exponents below 0 indicate stable dynamics (black line), whereas exponents above 0 indicate chaotic dynamics (red line). The vertical dashed line highlights the correspondence between the transition to chaos and the emergence of persistent activity by the two fixed-point attractor states.

two excitatory populations reflects the degree of 'perceptual evidence' of the strongly versus the weakly stimulated one (see methods). Hence, increasing the degree of perceptual evidence of one stimulus versus the other would correspond to an increase of the average stimulation for only one of the two populations, with the other staying at minimum baseline. Simulated trials consisted of evolving the system under such stochastic inputs for a duration of 1 s, and then classifying each trial as 'correct', 'incorrect', or 'no-decision' based on its final convergence—or non-convergence—and the actual stimulation values applied. We could already observe from simulated trials with equal perceptual evidence (figure 3(A)) that the overall decision-making dynamics (e.g., reaction times) changed with varying ACh levels. Moreover, we systematically characterized the behavior of the model by computing the corresponding psychometric functions—describing its performance—at different levels of perceptual evidence, ACh, and noise (figure 3(B)). We observed that at low ACh levels, the model did not converge to a decision, as shown by the high proportion of no-decision trials, or impasse. However, when the ACh level is increased to intermediate values, impasse trials are significantly reduced, and correct trials are in the majority. Higher values of ACh lead to a decrease of correct trials along with an increase of incorrect trials—or e.g., false alarms—at low perceptual evidence, especially with medium and high noise conditions. Thus, from these results, it follows that performance with similar or ambiguous stimuli would benefit from high levels of ACh—i.e., supercritical circuit—, as long as the noise is not strong enough to drive a hypersensitive—chaotic—circuit toward erroneous trajectories.

Subsequently, we analyzed the decision accuracy of the stochastic model with respect to the previously shown phase transition. To that end, we computed the proportion of correct trials at different combinations of the SST+/PV+ ratio—i.e., ACh level—and input noise, by averaging across perceptual evidence conditions

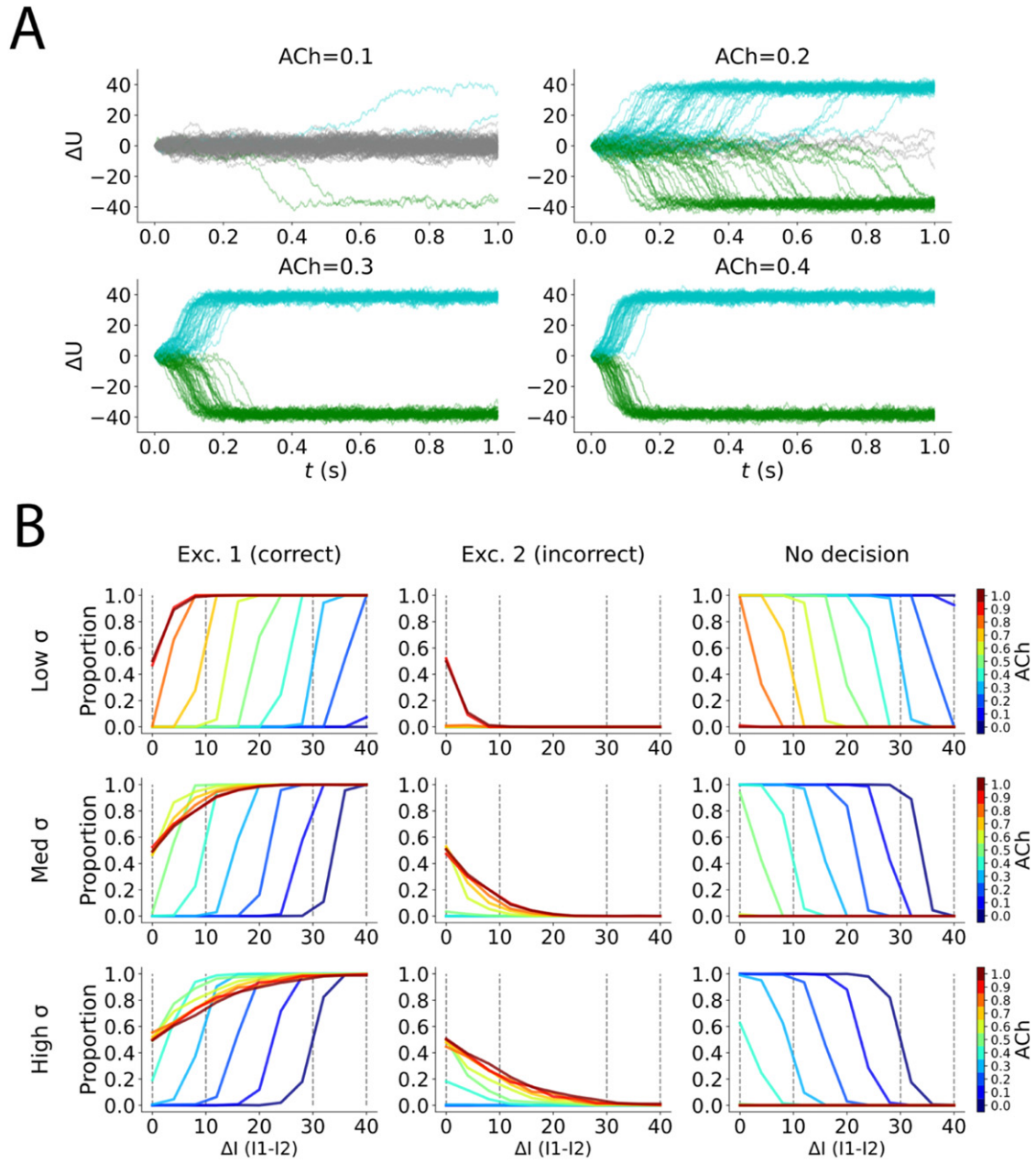

Figure 3. Performance trade-off between SST+/PV+ ratio and noise. (A) Examples of 100 trials with equal stimulation (i.e., unbiased) drawn from a range of ACh levels and with a medium level of noise. ΔU represents the difference in firing rate between the two populations. Gray lines represent no-convergence trials, and colored lines (cyan and green) represent the convergence of the model to one of the two attractor states. (B) Psychometric functions across the ACh range and for three different levels of noise. Correct choices were the ones where the model converged to the attractor biased by stimulation (i.e., perceptual evidence, or ΔI), whereas incorrect ones, or false alarms, occurred when the model reached the attractor with the weakest stimulation. No-decision trials, or impasse, are characterized by a lack of convergence to either attractor state. Rainbow coloring of lines denotes the range of ACh levels as shown in the color bars.

(see methods). The resulting accuracy peaks then correspond to the optimal ACh level across the input noise range (figure 4(A)). Interestingly, we observed a monotonic decrease of the optimal ACh level with increasing noise. This is explained by the previous observation that high input noise generates large fluctuations in the population dynamics and thus makes it easier for the circuit to fall into the weakest attractor. Thus, lowering the ACh level reduces the sensitivity of the circuit to its inputs and dampens the effects of large levels of noise. Finally, we estimated the phase transition in the stochastic model (and thus the edge-of-chaos regime) across the noise range by computing the proportion of no-decision trials during equal stimulation to both populations—i.e., unbiased stimuli, and thus, without perceptual evidence (figure 4(B)). Hence, a drop of no-decision trials would correspond to the emergence of persistent activity identified previously by the bifurcation diagram and the Lyapunov exponents (figure 2). Notably, the optimal ACh levels (from figure 4(A)) coincide with the edge-of-chaos regime. In conclusion, we observed that optimal decision-making across varying lev-

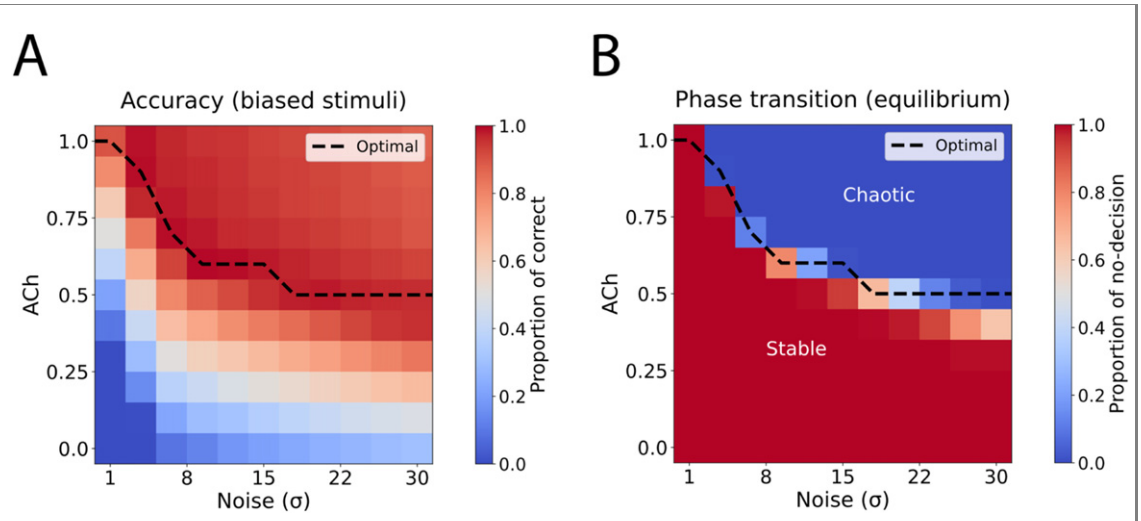

Figure 4. The optimal SST+/PV+ ratio coincides with the edge-of-chaos phase transition. (A) Performance of the model as the average proportion of correct trials across perceptual evidence conditions—simulating trials across the whole range of perceptual evidence (see methods). Simulations of the stochastic model were performed for different values of noise. Optimality (dashed line) is based on the ACh levels—SST+/PV+ ratio—achieving maximum accuracy (i.e., the proportion of correct trials) for a particular noise level, and thus it can be seen that the line follows the accuracy peaks across noise conditions (*x*-axis). (B) Putative phase transition from stability to chaos across noise levels as characterized by the consistent, sudden drop of no-decision trials for every noise condition. The dashed line (optimality) is mirrored from panel (A) and thus represents optimal accuracy, in order to show the correspondence between the optimal SST+/PV+ ratio and the edge-of-chaos.

els of perceptual evidence corresponds to the phase transition where supercritical dynamics—i.e., persistent activity—emerges.

3. Discussion

We addressed the question of how persistent activity can arise from attractor dynamics with inherent features of supercriticality—i.e., the tendency to generate long-lasting avalanches. Following previous distinctions between avalanche-based and edge-of-chaos criticality [23], we link the concept of edge-of-chaos with ignition-like supercritical states, to argue that optimal decision-making might occur at such a phase transition, where persistent activity emerges. In turn, we suggest that the SST+/PV+ gradient alone is sufficient to get the phase transition from critical and stable, to supercritical and chaotic dynamics.

First, we showed that, by modulating the SST+/PV+ ratio in our model, we could control the transition from a stable, low-firing regime to a chaotic regime with saturated persistent firing (figures 1 and 2). Next, we observed that moving beyond the edge-of-chaos into the chaotic regime impairs the performance of the model, especially under high input noise where random fluctuations dominate the temporal evolution of a hypersensitive circuit (figures 3 and 4(A)). Finally, by relating the model's performance under biased stimuli with its convergence dynamics under equilibrium—unbiased stimulation—, we showed, not only that the optimal SST+/PV+ ratio corresponds to the phase transition, but also that both decrease together, and monotonically, with input noise (figure 4). Hence, our results suggest that optimal decision-making lies at the edge-of-chaos, and that the SST+/PV+ ratio could further regulate such a phase transition depending on the input noise in order to attain optimal performance under dynamic uncertainty conditions.

The latter observation implies that the cortex might require regulation of its own intrinsic dynamics to account for the effects of varying input—or intrinsic—noise. Indeed, ACh, a neuromodulator that differentially modulates the firing of SST+ and PV+ interneurons [18], has been related to uncertainty estimation in the context of learning and plasticity [20]. Furthermore, cholinergic transients have been shown to increase the hits and false alarms in a signal detection task, suggesting a general effect of arousal or excitability [19]. These findings are consistent with our model and results (figure 3(B)), whereby ACh corresponds to a functional increase of the SST+/PV+ ratio, which in turn increases the input sensitivity of the circuit to random fluctuations, making it easier to converge to either attractor states—i.e., more false alarms. Therefore, based on our model's results, we suggest ACh release as a potential mechanism for the self-regulation of intrinsic population dynamics based on uncertainty estimates [20].

In addition, we note that our use of the edge-of-chaos transition differs from the classical notions of chaotic brain dynamics in an important respect [24, 25]. Whereas previous work has mostly focused on the role of chaotic attractors, aperiodic oscillations, and noise-induced first-order phase transitions [26], we introduce

Table 1. Parameters and variables of the model. Square brackets define a range of values; "a.u." stands for arbitrary units.

Parameter/variable	Description	Values	Units
U_i	Mean firing rate of excitatory population i (state variable in equations (1) and (2))	0 at $t = 0$	Hz
τ	Time constant determining the timescale of population dynamics	20	ms
w_+	Recurrent weight of excitatory populations	5	a.u.
w_-	Weight of mutual inhibition (SST+ interneurons)	4	a.u.
$w_=$	Weight of feedback inhibition (PV+ interneurons)	4	a.u.
Q	SST+/PV+ ratio, or ACh level, regulating mutual and feedback inhibition	[0, 1]	a.u.
I_i	External stimulation to excitatory population i	[4, 44]	Hz
σ	Variance of the Gaussian noise provided to the excitatory populations	[1, 30]	Hz
$\xi(t)$	Gaussian noise source	$\sim N(0, 1)$	a.u.
$F_{\max}$	Maximum firing rate of the population f–I logistic curve (equation (3))	40	Hz
k	Gain parameter of the f–I curve, setting the dynamic range	1/22	a.u.
θ	Threshold parameter of the f–I curve, setting the sigmoid's midpoint	15	Hz

chaos as the consequence of a saddle-node bifurcation enabling persistent activity. Indeed, the emergence of a saddle node in-between the fixed-point attractors inevitably renders the dynamics around the initial point (prior to the actual choice) chaotic. Hence, the emergence itself of persistent activity (the critical-to-supercritical phase transition) underlying decision-making is suggested to be tied to the emergence of chaotic dynamics (edge-of-chaos) by virtue of a saddle-node bifurcation—this relationship is well illustrated in figure 2.

Finally, the sudden emergence of supercritical dynamics underlying persistent activity with increasing SST+/PV+ ratio is consistent with the fact that such processes occur in higher-order areas like the prefrontal cortex, where it has been observed that the SST+/PV+ ratio is higher than in lower-order areas, such as $V1$ or $V4$ [10, 13]. Thus, it seems that the increasing SST+/PV+ gradient along the cortical hierarchy is sufficient to explain such distinct intrinsic dynamics and functional specialization of higher- and lower-order cortical sites. Overall, our results provide a plausible explanation of how the SST+/PV+ gradient across the cortical hierarchy could interact with neuromodulators—like ACh—to determine the function and dynamics of local cortical circuits.

4. Methods

We simulated the activity of two competing excitatory populations during a perceptual decision-making task with a variant of the canonical attractor model of the prefrontal cortex [21]. Concretely, we included the effects of the SST+ and PV+ interneurons as mutual and shared feedback inhibition, respectively. We did so by modifying the Wilson–Cowan equations [27] following [28], such that,

$$\tau \frac{\mathrm{d}U_1(t)}{\mathrm{d}t} = -U_1 + f\left(w_+ U_1 + I_1 - Q w_- U_2 - (1-Q)\, w_= f\left(U_1 + U_2\right)\right) + \sigma\xi(t) \tag{1}$$

$$\tau \frac{\mathrm{d}U_2(t)}{\mathrm{d}t} = -U_2 + f\left(w_+ U_2 + I_2 - Q w_- U_1 - (1-Q)\, w_= f\left(U_1 + U_2\right)\right) + \sigma\xi(t), \tag{2}$$

where $f\,(x)$ is the logistic f–I function,

$$f\,(x) = \frac{F_{\max}}{1 + \mathrm{e}^{\frac{-(x-\theta)}{k}}}. \tag{3}$$

A description of all the variables and parameters is provided below in table 1.

In contrast to previous studies, our model complements the direct mutual inhibition between the two excitatory populations with shared feedback inhibition based on a nonlinear integration of the overall activity of both populations. Thus, this feature makes feedback inhibition independent from the excitatory (recurrency) and mutual inhibition terms, allowing for the differential modulation of both inhibitory sources. Such differential modulation was captured in the model by the trade-off factor Q in equations (1), and (2)—and referred throughout the article as ACh or SST+/PV+ ratio, interchangeably.

The ordinary differential equations (ODEs)—equations (1) and (2), without the stochastic term $\sigma\xi(t)$—were used for figures 1 and 2 and were numerically integrated through time via the *lsoda* solver. In contrast, the stochastic differential equations—equations (1) and (2), with the stochastic term $\sigma\xi(t)$—were used for figures 3 and 4 (perceptual decision-making task) and were solved via the Euler–Maruyama algorithm for Ito equations. Stable and unstable stationary points of equations (1)–(3) were identified from the Jacobian matrix and the signs of the two corresponding eigenvalues—two negative values for fixed-point attractors, and one positive and one negative value for saddle nodes. To characterize the sensitivity of the circuit to small fluctuations around the starting point—chaotic dynamics—, the largest Lyapunov exponents (figure 2(B))

were computed using the Jacobian matrix and following the variational matrix method described in [29]. In addition, the bifurcation diagram (figure 2(A)) was obtained by extracting the last states after evolving the system for 1 s from 100 initial values, conforming a 0.01 × 0.01 rectangular grid with the origin (0, 0) as the lower-left corner of such a grid.

Task description. The perceptual decision-making task, which incorporates the stochastic inputs to both excitatory populations, was modeled by simulating state trajectories (examples in figure 3(A)) with different amounts of perceptual evidence (ΔI figure 3(B)). In turn, evidence was modeled as one population receiving constant minimal stimulation (4 Hz) while the other receiving equal or higher external stimulation (ranging from 4 to 44 Hz). Each trial consisted of 1 s of simulated activity, after which the last mean firing rate values of the two populations were compared. Then, the winner population (U_1 or U_2) was decided based on the difference between the firing rates (ΔU, or $U_1 - U_2$) surpassing the thresholds $F_{\max}/2$ or $-F_{\max}/2$. Correct and incorrect choices were then calculated as the proportions of trials that ended with either the strongly or the weakly stimulated population being the winner, respectively. In addition, no-decision (or impasse) trials were identified when $-F_{\max}/2 < \Delta U < F_{\max}/2$, and hence no convergence to either fixed-point attractor was reached. The steep decrease of the proportion of no-decision trials was used as an approximation—in the stochastic condition—of the previously observed saddle-node bifurcation leading to persistent activity in the deterministic model (figure 2), and therefore, to identify the phase transition from stability to chaos under realistic noisy stimulation (figure 4(B)).

Acknowledgments

This research was supported by the European Commission Horizon 2020 Grant Virtual Brain Cloud (number 826421), and by an FI-AGAUR scholarship to AFA from the Generalitat de Catalunya.

Data availability statement

The data that support the findings of this study are available upon reasonable request from the authors.

ORCID iDs

Adrián F Amil https://orcid.org/0000-0002-7164-4597
Paul F M J Verschure https://orcid.org/0000-0003-3643-9544

References

[1] Williams-García R V, Moore M, Beggs J M and Ortiz G 2014 Quasicritical brain dynamics on a nonequilibrium Widom line *Phys. Rev.* E **90** 062714
[2] Shew W L and Plenz D 2013 The functional benefits of criticality in the cortex *Neuroscientist* **19** 88–100
[3] Shew W L, Yang H, Yu S, Roy R and Plenz D 2011 Information capacity and transmission are maximized in balanced cortical networks with neuronal avalanches *J. Neurosci.* **31** 55–63
[4] Shew W L, Yang H, Petermann T, Roy R and Plenz D 2009 Neuronal avalanches imply maximum dynamic range in cortical networks at criticality *J. Neurosci.* **29** 15595–600
[5] Ma Z, Turrigiano G G, Wessel R and Hengen K B 2019 Cortical circuit dynamics are homeostatically tuned to criticality *in vivo* *Neuron* **104** 655–64
[6] Avramiea A-E, Masood A, Mansvelder H D and Linkenkaer-Hansen K 2021 Amplitude and phase coupling optimize information transfer between brain networks that function at criticality *bioRxiv Preprint* http://dx.doi.org/10.1101/2021.03.15.435461 (accessed 26 June 2021)
[7] Li M, Han Y, Aburn M J, Breakspear M, Poldrack R A, Shine J M and Lizier J T 2019 Transitions in information processing dynamics at the whole-brain network level are driven by alterations in neural gain *PLoS Comput. Biol.* **15** e1006957
[8] Curtis C E and Lee D 2010 Beyond working memory: the role of persistent activity in decision making *Trends Cogn. Sci.* **14** 216–22
[9] Curtis C E and D'Esposito M 2003 Persistent activity in the prefrontal cortex during working memory *Trends Cogn. Sci.* **7** 415–23
[10] Van Vugt B, Dagnino B, Vartak D, Safaai H, Panzeri S, Dehaene S and Roelfsema P R 2018 The threshold for conscious report: signal loss and response bias in visual and frontal cortex *Science* **360** 537–42
[11] Wang X-J 1999 Synaptic basis of cortical persistent activity: the importance of NMDA receptors to working memory *J. Neurosci.* **19** 9587–603
[12] Wang M, Yang Y, Wang C-J, Gamo N J, Jin L E, Mazer J A, Morrison J H, Wang X-J and Arnsten A F T 2013 NMDA receptors subserve persistent neuronal firing during working memory in dorsolateral prefrontal cortex *Neuron* **77** 736–49
[13] Wang X-J 2020 Macroscopic gradients of synaptic excitation and inhibition in the neocortex *Nat. Rev. Neurosci.* **21** 169–78
[14] Atallah B V, Bruns W, Carandini M and Scanziani M 2012 Parvalbumin-expressing interneurons linearly transform cortical responses to visual stimuli *Neuron* **73** 159–70
[15] Urban-Ciecko J and Barth A L 2016 Somatostatin-expressing neurons in cortical networks *Nat. Rev. Neurosci.* **17** 401–9

[16] Kim R and Sejnowski T J 2020 Strong inhibitory signaling underlies stable temporal dynamics and working memory in spiking neural networks *Nat. Neurosci.* **24** 129–39
[17] Lagzi F, Bustos M C, Oswald A-M and Doiron B 2021 Assembly formation is stabilized by Parvalbumin neurons and accelerated by Somatostatin neurons *bioRxiv Preprint* http://dx.doi.org/10.1101/2021.09.06.459211 (accessed 7 September 2021)
[18] Kawaguchi Y 1997 Selective cholinergic modulation of cortical GABAergic cell subtypes *J. Neurophysiol.* **78** 1743–7
[19] Gritton H J, Howe W M, Mallory C S, Hetrick V L, Berke J D and Sarter M 2016 Cortical cholinergic signaling controls the detection of cues *Proc. Natl Acad. Sci. USA* **113** E1089–97
[20] Puigbò J-Y, Arsiwalla X D, González-Ballester M A and Verschure P F M J 2020 Switching operation modes in the neocortex via cholinergic neuromodulation *Mol. Neurobiol.* **57** 139–49
[21] Wang X-J 2002 Probabilistic decision making by slow reverberation in cortical circuits *Neuron* **36** 955–68
[22] Albantakis L and Deco G 2011 Changes of mind in an attractor network of decision-making *PLoS Comput. Biol.* **7** e1002086
[23] Kanders K, Lorimer T and Stoop R 2017 Avalanche and edge-of-chaos criticality do not necessarily co-occur in neural networks *Chaos* **27** 47408
[24] Tsuda I 2001 Toward an interpretation of dynamic neural activity in terms of chaotic dynamical systems *Behav. Brain Sci.* **24** 793–810
[25] Skarda C A and Freeman W J 1987 How brains make chaos in order to make sense of the world *Behav. Brain Sci.* **10** 161–73
[26] Freeman W J 2011 Noise-induced first-order phase transitions in chaotic brain activity *Int. J. Bifurcation Chaos* **09** 2215–8
[27] Wilson H R and Cowan J D 1972 Excitatory and inhibitory interactions in localized populations of model neurons *Biophys. J.* **12** 1–24
[28] Marcos E, Pani P, Brunamonti E, Deco G, Ferraina S and Verschure P 2013 Neural variability in premotor cortex is modulated by trial history and predicts behavioral performance *Neuron* **78** 249–55
[29] Sandri M 1996 Numerical calculation of Lyapunov exponents *Math. J.* **6** 78–84